HHS Public Access

Author manuscript

Ultrasound Med Biol. Author manuscript; available in PMC 2017 February 01.

Published in final edited form as:

Ultrasound Med Biol. 2016 February ; 42(2): 528–538. doi:10.1016/j.ultrasmedbio.2015.09.017.

The dynamic behavior of microbubbles during long ultrasound tone-burst excitation: mechanistic insights into ultrasound-microbubble mediated therapeutics using high-speed imaging and cavitation detection

Xucai Chen[#], **Jianjun Wang**[#], **John J. Pacella**, and **Flordeliza S. Villanueva**

Center for Ultrasound Molecular Imaging and Therapeutics, University of Pittsburgh Medical Center, Pittsburgh, PA 15213, USA

[#] These authors contributed equally to this work.

Abstract

Ultrasound (US)-microbubble (MB) mediated therapies have been shown to restore perfusion and enhance drug/gene delivery. Due to the presumption that MBs do not persist during long US exposure under high acoustic pressures, most schemes utilize short US pulses when a high US pressure is employed. However, we recently observed an enhanced thrombolytic effect using long US pulses at high acoustic pressures. Therefore we explored the fate of MBs during long tone-burst exposures (5 ms) at various acoustic pressures and MB concentrations via direct high-speed optical observation and passive cavitation detection. MBs first underwent stable or inertial cavitation depending on the acoustic pressure, and then formed gas-filled clusters that continued to oscillate, break up, and form new clusters. Cavitation detection confirmed continued, albeit diminishing acoustic activity throughout the 5-ms US excitation. These data suggest that persisting cavitation activity during long tone-bursts may confer additional therapeutic effects.

Keywords

Microbubble Dynamics; Ultrasound Therapy; Ultrasound Contrast Agents; Sonothrombolysis; Cavitation; High-Speed Imaging

INTRODUCTION

Accumulating evidence suggest that intravenously injected microbubble (MB)-based ultrasound (US) contrast agents in conjunction with US delivery may have therapeutic effects, for restoring microvascular perfusion during acute myocardial infarction or stroke (Meairs and Culp 2009; Porter 2009) and enhancing drug or gene delivery for tumor

Corresponding author: Dr. Flordeliza S. Villanueva, Center for Ultrasound Molecular Imaging and Therapeutics, Heart and Vascular Institute, A351 PUH, 200 Lothrop Street, Pittsburgh, PA 15213, Phone: 412-647-5840, Fax: 412-647-4227, villanuevafs@upmc.edu, Website: www.imagingtherapeutics.pitt.edu.

suppression or tissue regeneration (Klibanov 2006; Ferrara et al. 2007; Newman and Bettinger 2007; Chen et al. 2010; Ibsen et al. 2013; Sutton et al. 2013; Lentacker et al. 2014; Chen et al. 2015). MB cavitation induced by US is thought to be a major mechanism of sonothrombolysis, where clot disruption is accelerated by US activated MBs through direct mechanical force (Kim et al. 2012; Chen et al. 2014) or enhanced material transport (Datta et al. 2008). MB cavitation is also mechanistically involved in sonoporation, where transient pores in the plasma membrane are formed to allow therapeutic loads to cross the cell membrane (Qin et al. 2014). Under varying experimental conditions, both stable and inertial cavitation regimes have been successful in studies of US-MB mediated clot disruption (Francis et al. 1992; Lauer et al. 1992; Blinc et al. 1993; Harpaz et al. 1993; Harpaz et al. 1994; Datta et al. 2006; Prokop et al. 2007; Datta et al. 2008; Leeman et al. 2012; Chen et al. 2014; Wu et al. 2014; Bader et al. 2015; Pacella et al. 2015) and gene or drug delivery (Frenkel et al. 2002; Pislaru et al. 2003; van Wamel et al. 2006; Carson et al. 2011; Carson et al. 2012; Escoffre et al. 2013; Fan et al. 2013; De Cock et al. 2014; Qin et al. 2014).

Stable cavitation is characterized by the sustained small amplitude oscillations of the MB (Flynn 1964), which generates local flow patterns termed microstreaming. The presence of MB acoustic emissions at the subharmonic frequency in response to US has been used to identify stable cavitation behavior (Bader and Holland 2013). Inertial cavitation is characterized by the collapse of the MB following a large expansion phase (Leighton 1994), is a transient process, and emits a broadband noise that can be the basis for its detection. Smaller MBs can be formed during inertial cavitation and these smaller daughter bubbles can serve as cavitation nuclei (Tu et al. 2006a; Tu et al. 2006b). It has been hypothesized that the transient nature of inertial cavitation may limit therapeutic bioeffects due to early destruction of the MBs, as compared to the longer-lived stable cavitation, which putatively promotes prolonged mixing and enhance transport of therapeutic agents (Bader et al. 2015).

Due to the presumption that MBs do not persist during long US exposure under high acoustic pressure, most US-mediated therapeutic schemes utilize a short US pulses (a few acoustic cycles or μs duration) when a high US pressure is used. However, we have recently observed enhanced thrombolytic effect *in vitro* using MBs and very long US pulses (up to 5000 cycles) at high acoustic pressures (Leeman et al. 2012). Therefore, we sought to explore the actual fate of MBs during a long acoustic cycle exposure by direct visual observation of MB acoustic behaviors at varying time points during a long tone-burst excitation. Such capability was conferred by the availability of an ultra-high speed camera to image MB oscillations in response to US (Chen et al. 2013). Passive cavitation detection (PCD) was used to study the cavitation activity throughout the long tone-burst excitation.

MATERIALS AND METHODS

Experimental Apparatus

A simplified schematic diagram of the experimental apparatus is shown Figure 1a. The system comprised a multi-frame high speed camera, a custom microscope (BXFM, Olympus Corp, Tokyo, Japan) an US and optical imaging chamber (Figure 1b), an US delivery system, and a passive cavitation detector.

High-speed imaging—A high-speed imaging system (UPMC Cam), described in detail previously (Chen et al. 2013), was used to acquire movies of oscillating MBs. Using a gas turbine powered by compressed helium to drive a rotating mirror, this system is capable of imaging microscopic movies at 25 million frames per second (Mfps) for 128 frames, with a maximum frame size of 920×616 pixels. A strobe light (MVS-700, PerkinElmer, Salem, MA) triggered from the camera system timing board served as the light source for bright field imaging.

Ultrasound and optical imaging chamber—A custom combined US and optical imaging chamber housed the US transmitter and receiver and allowed simultaneous acoustic and optical observation (Fig. 1b). A cellulose hollow fiber with a 200-μm inner diameter (Apectra/Por, Spectrum Laboratories, Inc., Rancho Dominguez, CA) was used to hold the sample. The imaging chamber was filled with degassed, deionized water and fitted on the microscope stage such that the US focus co-localized with the optical focus of the microscope.

Ultrasound delivery—US was delivered with a focused single element immersion transducer (A302S-SU-F1.63-PTF, Olympus NDT, Waltham, MA; center frequency 1 MHz, focal length 42.5 mm, −3 dB beam diameter at the focal plan 2.5 mm). A radio frequency (RF) tone-burst was generated with an arbitrary function generator (AFG3252, Tektronix, Beaverton, OR), triggered from the high speed imaging system, and amplified by a gated RF power amplifier (Model 250A250AM8, Amplifier Research, Souderton, PA) before it was sent to drive the US transmitter. The US field was calibrated with a 200-mm capsule hydrophone (HGL-0200, Onda Corp, Sunnyvale, CA). Long US tone-bursts of 5 ms duration (5,000 acoustic cycles) at 1 MHz and various peak negative pressures (0.25, 0.5, 1.0, and 1.5 MPa) were used to study the dynamic behavior of lipid MBs.

Passive cavitation detection—PCD was performed with a broadband focused single element immersion transducer (V326-SU-F1.00-PTF, Olympus NDT; center frequency 5 MHz, focal length 25.4 mm, −3 dB beam diameter at the focal plane 0.8 mm). The received RF signal was preamplified with an US pulse/receiver (5073PR, Olympus NTD, Waltham, MA) in receiver mode, filtered with a band pass filter (3–30 MHz), and digitized with a high resolution digitizer (Acqiris DP310, Agilent, Santa Clara, CA; 12 bits, 50 MHz). Joint time-frequency analysis of the digitized RF signal was performed with a window size of 1000 points (corresponding to 20 ms) and a 250-point increment step size (resulting in 75% overlap). A Hamming window was applied to the RF signal before digital Fourier transformation. Power averaging of the spectrograms of 10 RF traces was used for all samples in each experimental group. The mean power in the frequency band of 4.2–4.8 MHz was defined as the inertial cavitation strength (ICS) and the running cumulative value of ICS over time was defined as the inertial cavitation dose (ICD). It should be noted that the definition of ICS used here corresponds to the spectral power of the inertial cavitation activity, proportional to the squared value of the root-mean-squared (RMS) voltage from broadband noise used originally (Everbach et al. 1997). Using our definition, ICD is directly proportional to the energy associated with inertial cavitation.

Microbubble preparation

Perfluorobutane gas lipid-encapsulated MBs were prepared as previously described (Leeman et al. 2012). Briefly, a mixture of distearoyl-*sn*-glycero-3-phosphocholine, distearoyl-*sn*-glycero-3-phosphoethanolamine, and polyethylene glycol were sonicated in the presence of perfluorobutane gas to produce MBs with mean diameter of 3 μm and a concentration of 1×10^9 MBs/ml. MBs were diluted in equilibrated, gas-saturated saline to the desired concentration (2×10^6, 2×10^7, and 2×10^8 MB/ml) before being loaded to the cellulose tubing in the imaging chamber. With these concentrations, the number of MBs in the length of tubing imaged with a 10× objective (in and out of optical focal plane) was approximately 40, 400, and 4000, respectively.

Study protocol

MB behaviors were observed optically and acoustically during long US tone-burst excitation, at various acoustic pressures and MB concentrations. MB concentration may influence the fate of MB dynamics during long tone-burst excitation and hence the strength and duration of cavitation activity. A new MB suspension was infused into the cellulose tubing for each data acquisition. External flow was stopped during data acquisition. At an imaging rate of 5 Mfps or more, and with only 128 frames available for a given capture (i.e. less than 25.6 μs capture duration), our camera system cannot capture MB activity over an entire 5000 cycle tone-burst at 1 MHz (5 ms) in a single acquisition. Therefore, the US system was triggered such that MB activity at various tone-burst depths (0–5 ms) was captured, allowing observations of MB behavior at varying time points into the US pulse. Optical imaging was repeated 5 times at each time point for each peak negative pressure (0.25, 0.5, 1.0, and 1.5 MPa) and MB concentration (2×10^6, 2×10^7, and 2×10^8 MB/ml). Low optical magnification (10×) and a low frame rate (5 Mfps) were used to observe a relatively large field of MB behaviors over a relatively long period of time (25.6 μs), while higher magnification (60×) was used to observe MB oscillations in more detail. PCD was employed to record the scattered emissions for spectral analysis during the entire 5 ms tone-burst.

RESULTS

High-speed optical observations of MB fate during long US tone-burst excitation

Online supplemental high-speed movies 1–5 demonstrate typical MB behaviors (peak acoustic pressure 1.5 MPa, 2×10^7 MB/ml) at different time points during 5 ms US excitation pulses. MBs oscillated with large amplitude and started to move from right to left due to radiation force within the first few acoustic cycles (movie 1); At 0.1 ms, some MB clusters had formed near the tubing wall containing the MB suspension, and additional MBs continued to form clusters (movie 2). At 1 ms (movie 3), 3 ms (movie 4), and 5 ms (movie 5), only MB clusters could be observed. These MB clusters persisted and continued to oscillate with large amplitude throughout the 5 ms duration of the tone-burst.

Figures 2–4 are still frames from the high speed movies, showing the fate of the MBs at different time points during 5ms of US excitation at acoustic pressures of 0.25 MPa, 0.50 MPa, 1.0 MPa, and 1.5 MPa (panels a-d respectively) at concentrations of 2×10^6 MB/ml, 2×10^7 MB/ml and 2×10^8 MB/ml (Figures 2, 3, 4 respectively). Only one frame of each

movie is displayed, chosen at approximately the maximum expansion of the MBs or MB clusters.

At an MB concentration of 2×10^6 MB/ml (Figure 2), the amplitude of the oscillations increased as a function of acoustic pressure, as seen in the first column. At low acoustic pressure (0.25 MPa, Figure 2a), MB clusters formed slowly over time. At 0.1 ms, a combination of MB clusters and individual MBs was observed; at 1 ms and beyond, very few individual MBs were observed. At higher pressure (0.5 MPa, Figure 2b), both MB clusters and individual MBs were observed at 0.1 ms but only MB clusters were observed beyond 0.1 ms. At even higher acoustic pressures (1.0 MPa, Figure 2c and 1.5 MPa, Figure 2d), only MB clusters were observed at and beyond 0.1 ms. Note that MBs or daughter bubbles (Tu et al. 2006a; Tu et al. 2006b) persisted, formed clusters, and continued to oscillate well beyond 0.1 ms (100 cycles of US). The locations and the number of the clusters varied during each acquisition. Typically, only 0–4 clusters were observed in the image window at later time points.

At a higher MB concentration of 2×10^7 MB/ml (Figure 3 and online supplemental movies 1–5), a similar pattern was observed. However, the individual MBs persisted longer, especially at low acoustic pressure (Figure3a), the number of clusters increased, and they persisted longer into the duration of the 5 ms pulse. At the highest acoustic pressure studied, MB clusters were sometimes observed at 5 ms.

MB activities at the highest MB concentration (2×10^8 MB/ml) are shown in Figure 4. For a low acoustic pressure of 0.25 MPa (Figure 4a), individual MBs could still be observed even at 5 ms. As acoustic pressure increased, the number of individual MBs at a given time point progressively decreased relative to that at lower pressures (Figure 4b–d). At 1.5 MPa (Figure 4d), MB clusters of various sizes as well as individual MBs were observed at 1 ms.

MB cluster activity

Figure 5 displays sequential still frames of a high speed movie at 60× magnification of the continued formation of MB clusters 1 ms into a 5000 cycle tone-burst at 1.5 MPa peak negative pressure (see also online supplemental movie 6). The MB cluster continued to oscillate violently. At the largest expansion, the outer dimension of the MB cluster reached nearly 100 μm.

Cavitation detection

Figure 6 shows joint time-frequency analysis of the acoustic activity of MBs during the 5 ms US excitation at various acoustic pressures (rows a-d) for 2×10^6 MB/ml, 2×10^7 MB/ml and 2×10^8 MB/ml (Figure 6, columns 2–4, respectively). Background spectrograms without MBs are displayed as a reference (Figure 6, column 1). An 80 dB dynamic range was used for the spectral displays. At an MB concentration of 2×10^6 MB/ml (Figure 6, column 2), mostly stable cavitation was observed at 0.25 MPa, as indicated by the presence of subharmonic and ultraharmonic peaks and the relatively low level of broadband emissions throughout the 5 ms US excitation (Figure 6a, column 2; see also Figure 7a). At 0.5 MPa, both stable and inertial cavitation occurred, as indicated by the appearance of ultra-harmonics as well as broadband emissions (Figure 6b, column 2). At the beginning of the

tone-burst, more inertial cavitation was observed, as subharmonic and ultraharmonic peaks were barely visible. Later during the tone-burst, inertial cavitation decreased and subharmonic and ultraharmonic peaks became more apparent (see also Figure 7b). At 1.0 MPa, inertial cavitation dominated as broadband signal dominated in the center frequency band of the detector (Figure 6c, column 2). At 1.5 MPa, inertial cavitation persisted beyond 1 ms (Figure 6d, column 2), suggesting that the MB clusters concurrently seen on high speed imaging (Figure 2d) served as active cavitation nuclei and continued to undergo inertial cavitation. No ultraharmonic or subharmonic peaks were identified within the first 1 ms of US excitation (see also Figure 7d).

At a higher MB concentration of 2×10^7 MB/ml (Figure 6, column 3), a similar pattern was observed as for MB concentration of 2×10^6 but with higher spectral power. However, at a low acoustic pressure of 0.25 MPa (Figure 6a, column 3), stable cavitation persisted longer when compared with that for 2×10^6 MB/ml (Figure 6a, column 3). At higher acoustic pressures, inertial cavitation also lasted longer (Figure 6b–d, column 3) when compared with that for 2×10^6 MB/ml (Figure 6b–d, column 2).

At the highest MB concentration tested (2×10^8 MB/ml) (Figure 6, column 4), there was a delayed effect on maximum acoustic activities (see also Figure 8c), for both stable (Figure 6a, column 4) and inertial cavitation (Figure 6b–d, column 4). For a low acoustic pressure 0.25 MPa (Figure 6a, column 4), stable cavitation was observed throughout the 5 ms US excitation. At 1.5 MPa (Figure 6d, column 4), inertial cavitation was observed throughout the 5 ms US excitation, although most of the inertial cavitation occurred in the first millisecond.

Due to the very high dynamic range (80 dB) used to display the spectrograms in Figure 6, subtle differences in the spectral shape of the cavitation data were not clearly represented. The average power spectra during the first and second 0.25 ms of US exposure for a concentration of 2×10^6 MB/ml are plotted in Figure 7. Even though the transfer function of the PCD transducer was not corrected, subharmonic and ultraharmonic signals can still be observed. At 0.25 MPa (Figure 7a), stable cavitation was clearly present as evidenced by the subharmonic and ultraharmonic peaks in the first and second 0.25 ms of US exposure, with relatively low broadband content to the spectrum; at 0.5 MPa (Figure 7b), a combination of stable and inertial cavitation was observed, though inertial cavitation dominated the first 0.25 ms while stable cavitation was more apparent in the second 0.25 ms; at 1.0 MPa and 1.5 MPa (Figure 7c–d), the PCD signal was dominated by inertial cavitation such that subharmonic and ultraharmonic peaks could not be observed.

Inertial cavitation strength and dose

Figure 8 shows the mean ICS and cumulative ICD within the tone-burst as a function of time for MB concentrations of 2×10^6 MB/ml, 2×10^7 MB/ml and 2×10^8 MB/ml, respectively. Very low levels of inertial cavitation were observed at 0.25 MPa for any of the concentrations studied. ICS increased with pressure and MB concentration (Figure 8a–c), with most of the energy contained in the first millisecond. ICD increased with pressure and MB concentration (Figure 8d–f), and continued to rise as a function of time throughout the 5 ms US exposure. Figure 9 summarizes the total ICD resulting from the acoustic activity of

MBs during the 5 ms of US excitation at various acoustic pressures and concentrations. Total ICD increased with acoustic pressure for each MB concentration used ($p<0.05$) and increased with MB concentration for acoustic pressures at 0.5 MPa, 1.0 MPa and 1.5 MPa ($p<0.05$).

DISCUSSION

This study was motived by our previous finding that long US pulses (up to 5000 cycles) at high acoustic pressures enhanced the thrombolytic effect in an *in vitro* flow model (Leeman et al. 2012). MBs are not expected to persist during long acoustic cycles under high acoustic pressure. Once the MB shell integrity has been compromised, the gas pocket diffuses into the surrounding media. Little is known about the fate of the gas once liberated from the encapsulating lipid shell, especially when the US pulse duration is prolonged, and therefore, how it is possible for long tone-bursts to have increasing thrombolytic effect. Our current data indicate that during a long tone-burst–exposure, lipid shell encapsulated MBs first underwent stable or inertial cavitation, depending on the acoustic pressure, and survived as clusters that persisted and continued to oscillate with large amplitude.

The fate of MBs during US excitation

Our data provide the first direct optical confirmation that MBs or daughter bubbles can indeed persist (up to 5 ms) as clusters and remain acoustically active. MBs could not be seen after US exposure, which strongly suggests that the MB generating acoustic activity during the latter part of the tone-burst were not the original encapsulated MBs.

In early studies on the bioeffects of US with MB, it was observed that ultrasonic lysis of biological cells in suspension *in vitro* was facilitated or enhanced by rotation of the exposure vessel. Enhanced ultrasonic cell lysis due to rotation of the exposure vessel was observed at relatively high rotation speeds of tens to hundreds of rotations per minute (rpm) (Church et al. 1982; Sacks et al. 1982; Brayman and Miller 1992; Miller and Williams 1992), or only a few complete rotations of the exposure vessel during the exposure period (Carstensen et al. 1993). These studies suggest that MBs or the remnant cavitation nuclei survived US exposure for some time, being pushed to the side of the exposure vessel due to radiation force, and the rotation of the exposure vessel enhanced the mixing process of cells and MBs by recycling the cavitation nuclei. The bubble recycling hypothesis relevant to ultrasonic lysis *in vitro* was confirmed by exposure of stationary vessels to interleafed, opposing pulses of US (Brayman et al. 1994). In that study, opposing US pulses were used with pulse length varying from 50 μs to 5 s. It was optically shown that the smaller MBs generated during the breaking of a single MB continued to oscillate till the end of the 547 cycle excitation (Kokhuis et al. 2012). Our optical images of a population of MBs provide the first direct confirmation that MBs or their remnant daughter bubbles form clusters and continue to oscillate during long tone-burst US exposure--up to 5,000 acoustic cycles--at various MB concentrations and acoustic pressures (Figures 2–5).

The observations were made under non-flowing conditions. If we had chosen a flow system with axial flow velocity similar to that of blood velocity within arterioles at 2 mm/s, the axial motion of the external flow would carry the MBs by only 10 μm during the 5-ms pulse,

substantially smaller than the size of the observation window (325×599 μm). This axial flow velocity is much lower than the microbubble motion due to primary radiation force, on the order of 1 m/s. Therefore, no major difference in the observations was expected.

The therapeutic potential of long tone-burst

It has been suggested that ICD may have a direct correlation with US mediated therapeutic efficacy (Everbach et al. 1997; Chen et al. 2003a; Chen et al. 2003b; Datta et al. 2006). Specifically, the pulse length (from 5 to 200 cycles) dependence of ICD and cell lysis was investigated, and it was found that longer pulses (100 and 200 cycles) produced more ICD and more cell lysis (Chen et al. 2003a).

Our PCD data indicate that, for the range of MB concentrations considered, the duration of inertial cavitation persisted beyond what we had expected. At the highest concentration and acoustic pressure applied, inertial cavitation lasted well into 1000 acoustic cycles (Figure 6), much longer than the pulse durations employed in previous studies employing clinical US imaging systems (Frenkel et al. 2002) or single element transducers (Fan et al. 2013). ICD increased with acoustic pressure and MB concentration (Figure 8d–f) throughout the duration of the US exposure. Our data suggest that for therapy such as sonothrombolysis within the inertial cavitation regime, long pulses with durations of 100 cycles or longer could be used to harvest the therapeutic effect conferred by remnant bubbles as cavitation nuclei to sustain cavitation activity. These pulses can be separated in time by using relatively low pulse repetition frequency (PRF) to allow MB reperfusion into the treatment area and maintain acceptable levels of spatial peak-temporal average acoustic intensity (I_{SPTA}). For therapy within the stable cavitation regime, which has been shown to be more effective than inertial cavitation for sonothrombolysis in some reports (Datta et al. 2006), pulse durations of 1000 cycles or longer could be used, coupled with the appropriate PRF to maximize therapeutic efficiency and minimize undesirable effects such as heating for both *in vitro* and *in vivo* studies.

The effect of vessel size and MB concentration

We employed a 200-μm cellulose tube to confine the MBs for optical and acoustic observations, a phantom that is more relevant to the microvasculature than to larger vessels. In the present study, the use of spatial confinement would have reduced the effects of microstreaming (Starritt et al. 1989). Without this spatial confinement, MBs would have traveled out of the field of view for both optical and acoustic observations at the end of the 5 ms treatment for any of the acoustic pressures tested due to the primary Bjerknes force. It is possible that optical observation would fail to capture the prolonged existence of acoustically active MB clusters simply because they moved out of the optical field of view and PCD would fail to detect their prolonged cavitation signatures because they moved out of the co-focal area of the US transmitter and detector. In fact, a previous study was conducted to compare such exposure setups using US imaging and PCD (Mannaris and Averkiou 2012). It was found that for open exposure chambers, the movement of MBs out of the region of observation made it impossible to capture the true fate of MBs for long tone-burst excitations. However, Mannaris and colleagues observed longer cavitation activity in a 200-μm micro-tubing and recommended a 100-cycle pulse at MI>0.4 because pulses longer

than 100 cycle at high acoustic pressure did not produce added benefits in terms of MB oscillation. Our data for a 200-μm vessel indicate that up to 1000 cycles could be used to harvest the additional therapeutic potential of the MB activity. The optimal pulse duration can depend on the MB concentration and size of the vessel. In fact, we observed additional thrombolytic effect *in vitro* using 5,000 acoustic cycles (vs. 3,000 acoustic cycles) in a 4-mm vessel phantom (Leeman et al. 2012).

ICD as a measure of therapeutic potential increased with acoustic pressure and MB concentration (Figure 9). The time course of MB activity and ICD within the tone-burst depended on the combination of MB concentration and acoustic pressure (Figure 8). While the lower MB concentration studied (2×10^6 MB/ml and 2×10^7 MB/ml) can be achieved with an imaging dose and a therapeutic dose of contrast agents, respectively, the highest concentration studied (2×10^8 MB/ml) may not be achievable *in vivo*. However, over such a wide range of MB concentrations (100 fold), the general fate of the MBs during long US tone-burst excitation is similar: they persist as clusters and continue to oscillate; these oscillations contribute to ICD to provide potential therapeutic effect.

MB cluster spacing

From Figures 2–4 and the online movies 1–5, there appears to be a spatial periodicity of the MB cluster locations. We point out that it is unlikely that the spacing of the clusters was caused by standing waves. The wavelength of the 1 MHz ultrasound in the test medium is approximately 1.5 mm while the spacing between the MB clusters is variable, between 100–300 μm. We hypothesize that the spacing is dynamically determined by a balance of primary and secondary acoustic radiation forces of the MB clusters. A theoretical investigation into this phenomenon is beyond the scope of the current study.

Study limitations

We used a 200-μm cellulose tubing to confine the MBs, which mimics the microcirculation better than the larger vessels. We used a PCD that was optimized for inertial cavitation detection. By choosing a transducer with a center frequency (5 MHz) higher than the treatment frequency (1 MHz), detected scattering signal from non-MB boundaries was reduced and broadband noise emission due to inertial cavitation was easily identified. As such, the fundamental and the subharmonic signals were reduced. Ideally, a PCD transducer with extra flat spectral response should be used (Prokop et al. 2007).

We did not address the fate of the lipid shell encapsulating the initial MBs during US exposure. It has been shown that the lipid material encapsulating the MBs can be shed due to US exposure (Borden et al. 2005; Kwan and Borden 2012; Luan et al. 2014). It is likely that the oscillating MBs observed during the latter part of the tone-burst (>1 ms) are unencapsulated since the acoustic pressures used were all above the rupture threshold of the lipid MBs and no MB could be observed after US was turned off for any of the pressure settings used for this study.

SUMMARY

Our data show for the first time with direct high-speed optical observation that MBs or their remnant daughter bubbles persist as clusters that continue to oscillate with large amplitude during a single long tone-burst. PCD further corroborated the longevity of MB activity. This discovery may explain why long acoustic cycles have superior therapeutic effect for US-MB mediated therapies such as sonothrombolysis compared to shorter pulses, and represents one strategy by which to optimize such therapies.

Supplementary Material

Refer to Web version on PubMed Central for supplementary material.

ACKNOWLEDGEMENTS

Dr. Villanueva is funded in part by the National Institutes of Health (R01EB016516-01A1). This work was funded in part by the Center for Ultrasound Molecular Imaging and Therapeutics, University of Pittsburgh Heart, Lung and Vascular Medicine Institute, Pittsburgh, PA. The project described was also supported by Grant Number UL l RR024153 from the National Center for Research Resources (NCRR), a component of the National Institutes of Health (NIH) and NIH Roadmap for Medical Research. The authors wish to thank Drs. Brandon Helfield and Francois Yu for helpful discussions.

REFERENCES

Bader KB, Gruber MJ, Holland CK. Shaken and stirred: mechanisms of ultrasound-enhanced ehrombolysis. Ultrasound Med Biol. 2015; 41:187–96. [PubMed: 25438846]

Bader KB, Holland CK. Gauging the likelihood of stable cavitation from ultrasound contrast agents. Physics Med Biol. 2013; 58:127–44.

Blinc A, Francis CW, Trudnowski JL, Carstensen EL. Characterization of ultrasound-potentiated fibrinolysis in vitro. Blood. 1993; 81:2636–43. [PubMed: 8490172]

Brayman AA, Azadniv M, Miller MW, Chen X. Bubble recycling and ultrasonic cell lysis in a stationary exposure vessel. J Acoust Soc Am. 1994; 96:627–33. [PubMed: 7930063]

Brayman AA, Miller MW. Bubble cycling and standing waves in ultrasonic cell lysis. Ultrasound Med Biol. 1992; 18:411–20. [PubMed: 1509616]

Carson AR, McTiernan CF, Lavery L, Grata M, Leng X, Wang J, Chen X, Villanueva FS. Ultrasound-targeted microbubble destruction to deliver siRNA cancer therapy. Cancer Res. 2012; 72:6191–9. [PubMed: 23010078]

Carson AR, McTiernan CF, Lavery L, Hodnick A, Grata M, Leng X, Wang J, Chen X, Modzelewski RA, Villanueva FS. Gene therapy of carcinoma using ultrasound-targeted microbubble destruction. Ultrasound Med Biol. 2011; 37:393–402. [PubMed: 21256666]

Carstensen EL, Kelly P, Church CC, Brayman AA, Child SZ, Raeman CH, Schery L. Lysis of erythrocytes by exposure to CW ultrasound. Ultrasound Med Biol. 1993; 19:147–65. [PubMed: 8516961]

Chen S, Chen J, Huang P, Meng XL, Clayton S, Shen JS, Grayburn PA. Myocardial regeneration in adriamycin cardiomyopathy by nuclear expression of GLP1 using ultrasound targeted microbubble destruction. Biochem Biophys Res Commun. 2015; 458:823–9. [PubMed: 25701791]

Chen S, Shimoda M, Wang MY, Ding J, Noguchi H, Matsumoto S, Grayburn PA. Regeneration of pancreatic islets in vivo by ultrasound-targeted gene therapy. Gene Ther. 2010; 17:1411–20. [PubMed: 20508600]

Chen WS, Brayman AA, Matula TJ, Crum LA. Inertial cavitation dose and hemolysis produced in vitro with or without Optison. Ultrasound Med Biol. 2003a; 29:725–37. [PubMed: 12754072]

Chen WS, Brayman AA, Matula TJ, Crum LA, Miller MW. The pulse length-dependence of inertial cavitation dose and hemolysis. Ultrasound Med Biol. 2003b; 29:739–48. [PubMed: 12754073]

Chen X, Leeman JE, Wang J, Pacella JJ, Villanueva FS. New insights into mechanisms of sonothrombolysis using ultra-high-speed Imaging. Ultrasound Med Biol. 2014; 40:258–62. [PubMed: 24139920]

Chen X, Wang J, Versluis M, de Jong N, Villanueva FS. Ultra-fast bright field and fluorescence imaging of the dynamics of micrometer-sized objects. Rev Sci Instrum. 2013; 84:063701. [PubMed: 23822346]

Church CC, Flynn HG, Miller MW, Sacks PG. The exposure vessel as a factor in ultrasonically-induced mammalian cell lysis--II. An explanation of the need to rotate exposure tubes. Ultrasound Med Biol. 1982; 8:299–309. [PubMed: 7101578]

Datta S, Coussios CC, Ammi AY, Mast TD, de Courten-Myers GM, Holland CK. Ultrasound-enhanced thrombolysis using Definity as a cavitation nucleation agent. Ultrasound Med Biol. 2008; 34:1421–33. [PubMed: 18378380]

Datta S, Coussios CC, McAdory LE, Tan J, Porter T, De Courten-Myers G, Holland CK. Correlation of cavitation with ultrasound enhancement of thrombolysis. Ultrasound Med Biol. 2006; 32:1257–67. [PubMed: 16875959]

De Cock I, Zagato E, Braeckmans K, Luan Y, de Jong N, De Smedt SC, Lentacker I. Ultrasound and microbubble mediated drug delivery: Acoustic pressure as determinant for uptake via membrane pores or endocytosis. J Control Release. 2014; 197C:20–8. [PubMed: 25449801]

Escoffre JM, Mannaris C, Geers B, Novell A, Lentacker I, Averkiou M, Bouakaz A. Doxorubicin Liposome-Loaded Microbubbles for Contrast Imaging and Ultrasound-Triggered Drug Delivery. IEEE Transactions on Ultrasonics Ferroelectrics and Frequency Control. 2013; 60:78–87.

Everbach EC, Makin IR, Azadniv M, Meltzer RS. Correlation of ultrasound-induced hemolysis with cavitation detector output in vitro. Ultrasound in Medicine & Biology. 1997; 23:619–24. [PubMed: 9232771]

Fan Z, Chen D, Deng CX. Improving ultrasound gene transfection efficiency by controlling ultrasound excitation of microbubbles. J Control Release. 2013; 170:401–13. [PubMed: 23770009]

Ferrara K, Pollard R, Borden M. Ultrasound microbubble contrast agents: fundamentals and application to gene and drug delivery. Annual Review of Biomedical Engineering. 2007; 9:415–47.

Flynn, HG. Physics of acoustic cavitation in liquids. In: Mason, WP., editor. Physical Acoustics. Academic Press; New York: 1964. p. 58-172.

Francis CW, Onundarson PT, Carstensen EL, Blinc A, Meltzer RS, Schwarz K, Marder VJ. Enhancement of fibrinolysis in vitro by ultrasound. J Clin Invest. 1992; 90:2063–8. [PubMed: 1430229]

Frenkel PA, Chen S, Thai T, Shohet RV, Grayburn PA. DNA-loaded albumin microbubbles enhance ultrasound-mediated transfection in vitro. Ultrasound Med Biol. 2002; 28:817–22. [PubMed: 12113794]

Harpaz D, Chen X, Francis C, Marder V, Meltzer R. Ultrasound enhancement of fibrinolysis and reperfusion in vitro. J Am Coll Cardiol. 1993; 21:1507–11. [PubMed: 8473663]

Harpaz D, Chen X, Francis C, Meltzer R. Ultrasound accelerates urokinase induced thrombolysis and reperfusion. Am Heart J. 1994; 127:1211–9. [PubMed: 8172048]

Ibsen S, Schutt CE, Esener S. Microbubble-mediated ultrasound therapy: a review of its potential in cancer treatment. Drug design, development & therapy. 2013; 7:375–88.

Kim JS, Leeman JE, Kagemann L, Yu FTH, Chen X, Pacella JJ, Schuman JS, Villanueva FS, Kim K. Volumetric quantification of in vitro sonothrombolysis with microbubbles using high-resolution optical coherence tomography. Journal of Biomedical Optics. 2012; 17:070502-1. [PubMed: 22894458]

Klibanov AL. Microbubble contrast agents: targeted ultrasound imaging and ultrasound-assisted drug-delivery applications. Investigative Radiology. 2006; 41:354–62. [PubMed: 16481920]

Kokhuis TJA, Luan Y, Mastik F, Beurskens RHSH, Versluis M, De Jong N. Segmented high speed imaging of vibrating microbubbles during long ultrasound pulses. IEEE International Ultrasonics Symposium (IUS). 2012:1343–6.

Lauer CG, Burge R, Tang DB, Bass BG, Gomez ER, Alving BM. Effect of ultrasound on tissue-type plasminogen activator-induced thrombolysis. Circulation. 1992; 86:1257–64. [PubMed: 1394932]

Leeman JE, Kim JS, Yu FTH, Chen X, Kim K, Wang J, Chen X, Villanueva FS, Pacella JJ. Effect of acoustic conditions on microbubble-mediated microvascular sonothrombolysis. Ultrasound Med Biol. 2012; 38:1589–98. [PubMed: 22766112]

Leighton, T. The Acoustic Bubble. Academic Press; San Diego: 1994.

Lentacker I, De Cock I, Deckers R, De Smedt SC, Moonen CTW. Understanding ultrasound induced sonoporation: Definitions and underlying mechanisms. Advanced Drug Delivery Reviews. 2014; 72:49–64. [PubMed: 24270006]

Mannaris C, Averkiou MA. Investigation of microbubble response to long pulses used in ultrasound-enhanced drug delivery. Ultrasound in Medicine & Biology. 2012; 38:681–91. [PubMed: 22341047]

Meairs S, Culp W. Microbubbles for thrombolysis of acute ischemic stroke. Cerebrovascular Diseases. 2009; 27(Suppl 2):55–65. [PubMed: 19372661]

Miller DL, Williams AR. Nucleation and evolution of ultrasonic cavitation in a rotating exposure chamber. J Ultrasound Med. 1992; 11:407–12. [PubMed: 1495132]

Newman CM, Bettinger T. Gene therapy progress and prospects: ultrasound for gene transfer. Gene Ther. 2007; 14:465–75. [PubMed: 17339881]

Pacella JJ, Brands J, Schnatz F, Chen X, Villanueva FS. Treatment of microvascular microembolization using microbubbles and long tone burst ultrasound: an in vivo study. Ultrasound Med Biol. 2015; 41:456–64. [PubMed: 25542487]

Pislaru SV, Pislaru C, Kinnick RR, Singh R, Gulati R, Greenleaf JF, Simari RD. Optimization of ultrasound-mediated gene transfer: comparison of contrast agents and ultrasound modalities. Eur Heart J. 2003; 24:1690–8. [PubMed: 14499233]

Porter TR. The utilization of ultrasound and microbubbles for therapy in acute coronary syndromes. Cardiovascular Research. 2009; 83:636–42. [PubMed: 19541670]

Prokop AF, Soltani A, Roy RA. Cavitational mechanisms in ultrasound-accelerated fibrinolysis. Ultrasound Med Biol. 2007; 33:924–33. [PubMed: 17434661]

Qin P, Xu L, Hu Y, Zhong W, Cai P, Du L, Jin L, Yu AC. Sonoporation-induced depolarization of plasma membrane potential: analysis of heterogeneous impact. Ultrasound Med Biol. 2014; 40:979–89. [PubMed: 24462155]

Sacks PG, Miller MW, Church CC. The exposure vessel as a factor in ultrasonically-induced mammalian cell lysis--I. A comparison of tube and chamber systems. Ultrasound Med Biol. 1982; 8:289–98. [PubMed: 7101577]

Starritt HC, Duck FA, Humphrey VF. An experimental investigation of streaming in pulsed diagnostic ultrasound beams. Ultrasound Med Biol. 1989; 15:363–73. [PubMed: 2527429]

Sutton JT, Haworth KJ, Pyne-Geithman G, Holland CK. Ultrasound-mediated drug delivery for cardiovascular disease. Expert Opinion on Drug Delivery. 2013; 10:573–92. [PubMed: 23448121]

Tu J, Hwang JH, Matula TJ, Brayman AA, Crum LA. Intravascular inertial cavitation activity detection and quantification in vivo with Optison. Ultrasound Med Biol. 2006a; 32:1601–9. [PubMed: 17045881]

Tu J, Matula TJ, Brayman AA, Crum LA. Inertial cavitation dose produced in ex vivo rabbit ear arteries with Optison by 1-MHz pulsed ultrasound. Ultrasound Med Biol. 2006b; 32:281–8. [PubMed: 16464673]

van Wamel A, Kooiman K, Harteveld M, Emmer M, ten Cate FJ, Versluis M, de Jong N. Vibrating microbubbles poking individual cells: drug transfer into cells via sonoporation. J Control Release. 2006; 112:149–55. [PubMed: 16556469]

Wu J, Xie F, Kumar T, Liu J, Lof J, Shi W, Everbach EC, Porter TR. Improved sonothrombolysis from a modified diagnostic transducer delivering impulses containing a longer pulse duration. Ultrasound Med Biol. 2014; 40:1545–53. [PubMed: 24613551]

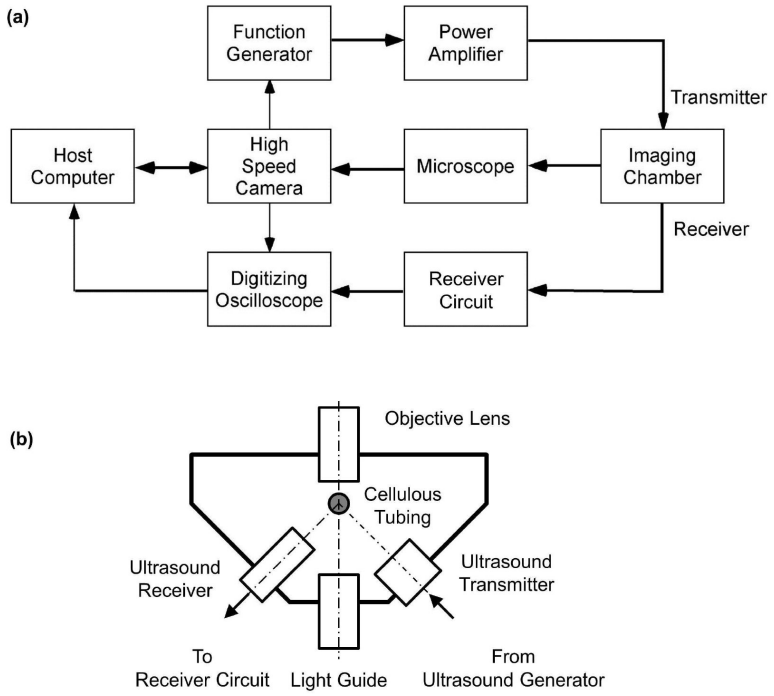

Figure 1.

(a) A simplified schematic diagram of the experimental apparatus. The system comprised a multi-frame high speed camera, a custom microscope, an US and optical imaging chamber, an US delivery system, and a passive cavitation detector. (b) A schematic diagram of the US and optical imaging chamber.

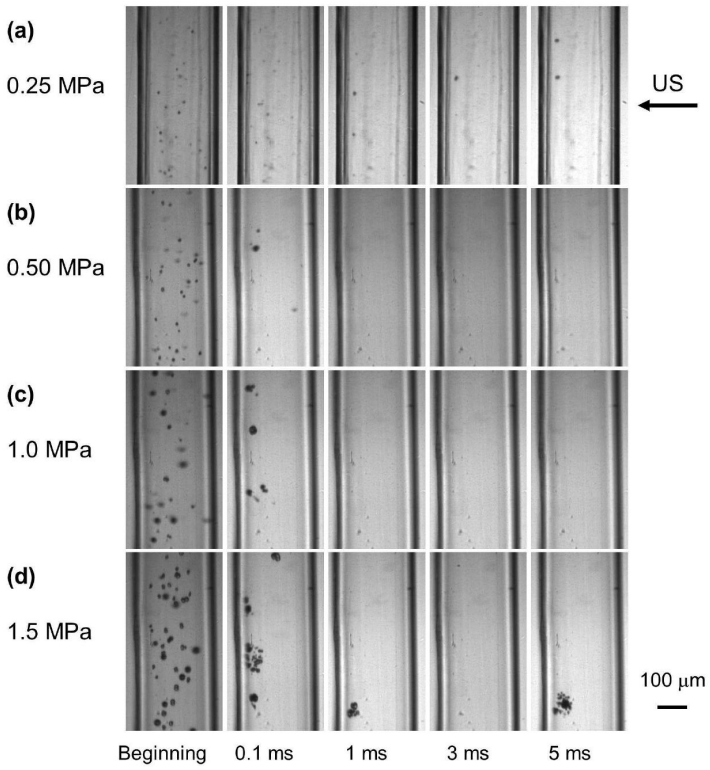

Figure 2.

The fate of lipid MBs during US excitation at different time points of a 5000 cycle treatment at various acoustic pressures at 2×10^6 MB/ml. Only one frame of each movie is displayed, chosen at approximately the maximum expansion of the MB or MB cluster. The frame size is 325×599 μm.

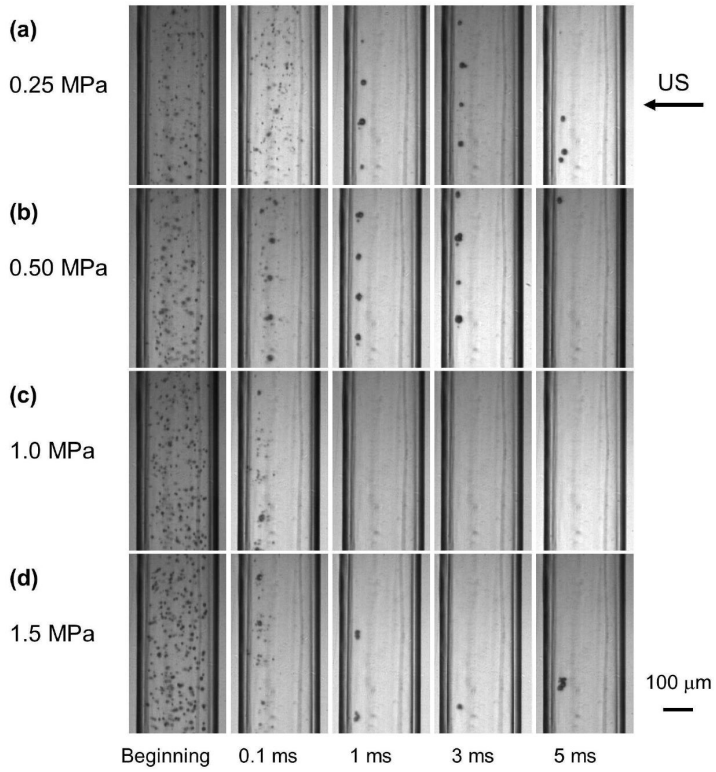

Figure 3.

The fate of lipid MBs during US excitation at different time points of a 5000 cycle treatment at various acoustic pressures at 2×10^7 MB/ml. The frame size is 325×599 μm. Also see online supplemental movies 1–5.

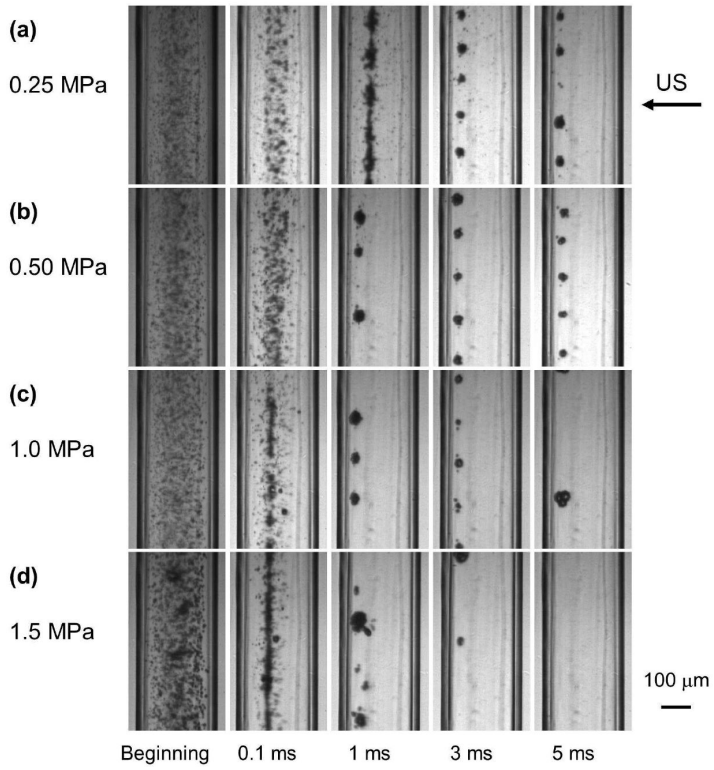

Figure 4.

The fate of lipid MB during US excitation at different time points of a 5000 cycle treatment at various acoustic pressures at 2×10^8 MB/ml. The frame size is 325×599 μm.

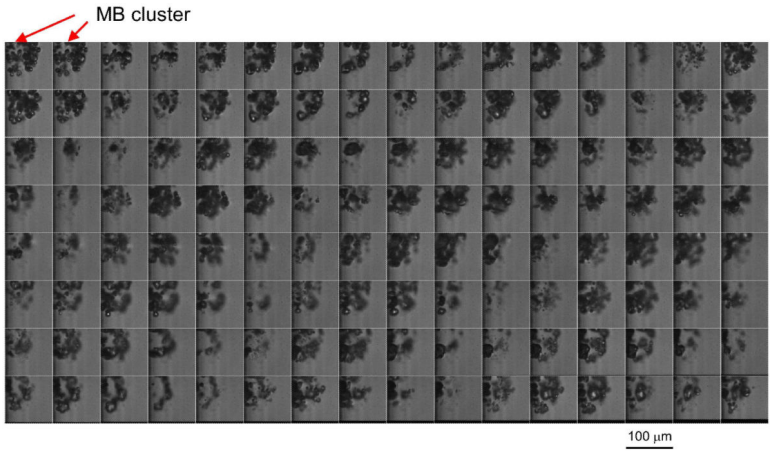

Figure 5.

Sequential still frames of high speed movie showing the detailed acoustic activity of a cluster of MBs 1,000 acoustic cycles into a long tone-burst (1.5 MPa, 1 MHz). For this example, the movie was taken at 5 Mfps with a 60× objective and the movie duration was 25.6 μs. The frame size is 100×100 μm. Also see supplemental movie 6.

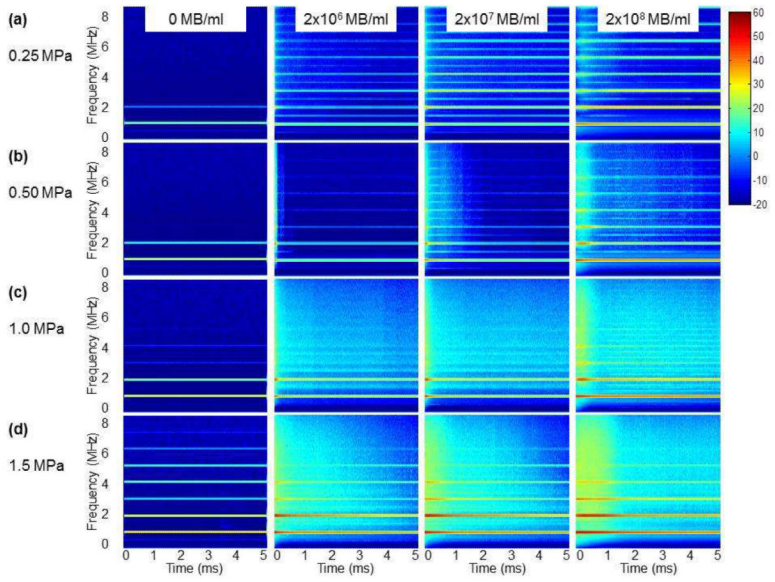

Figure 6.

Mean time-frequency spectra of the acoustic activity of lipid MBs during US excitation of a 5000 cycle treatment at various acoustic pressures and concentrations (*n*=10 for each setting). (a) 0.25 MPa; (b) 0.50 MPa; (c) 1.0 MPa; (d) 1.5 MPa. Column 1: No MB; Column 2: 2×10^6 MB/ml; Column 3: 2×10^7 MB/ml; Column 4: 2×10^8 MB/ml. Display dynamic range is 80 dB.

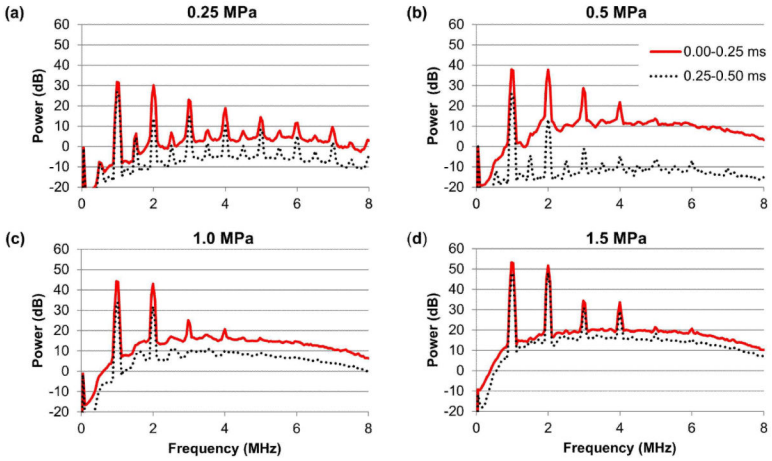

Figure 7.

Mean power spectra of the acoustic activity of lipid MBs at various acoustic pressures at 2×10^6 MB/ml during the first 250 acoustic cycles (solid red line) and the second 250 acoustic cycles (dashed black line) (n=10 for each setting). (a) 0.25 MPa, (b) 0.5 MPa, (c) 1.0 MPa, (d) 1.5 MPa.

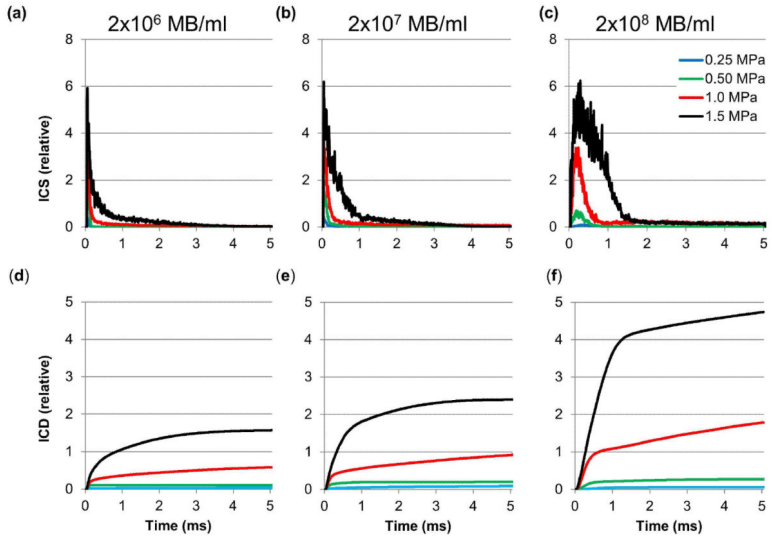

Figure 8.

Inertial cavitation strength (a–c) and cumulative inertial cavitation dose (d–f) of the acoustic activity of lipid MBs during 5 ms US excitation at various acoustic pressures at 2×10^6 MB/ml (a, d), 2×10^7 MB/ml (b, e), and 2×10^8 MB/ml (c, f), respectively (n=10 for each setting).

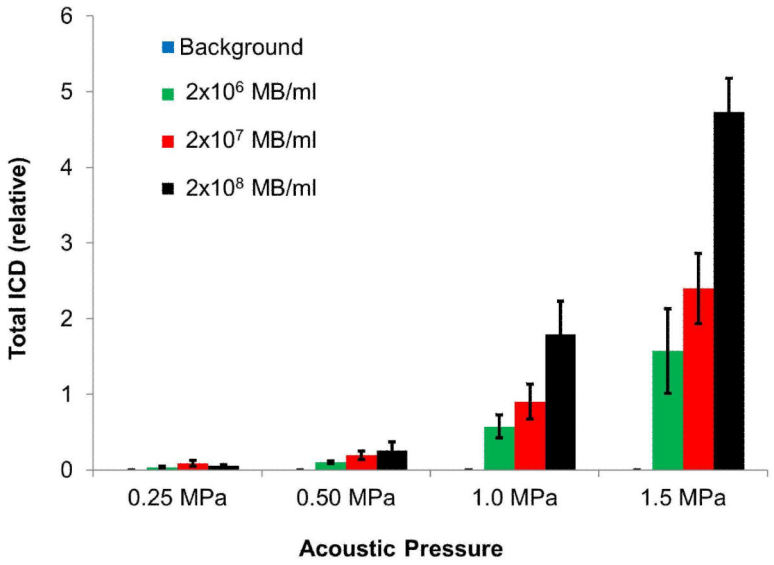

Figure 9.

Comparison of the cumulative inertial cavitation dose (mean ± standard deviation, *n*=10 for each setting) of the acoustic activity of lipid MBs during US excitation of a 5000 cycle treatment at various acoustic pressures and concentrations. Total ICD increased with acoustic pressure for each MB concentration used ($p<0.05$) and increased with MB concentration for acoustic pressures at 0.5 MPa, 1.0 MPa and 1.5 MPa ($p<0.05$).